

## Chain motion and viscoelasticity in highly entangled solutions of semiflexible rods

Shriram Ramanathan and David C Morse\*

*Department of Chemical Engineering and Materials Science,  
University of Minnesota, Minneapolis, MN 55455, USA*

(Dated: October 6, 2018)

Brownian dynamics simulations are used to study highly entangled solutions of semiflexible polymers. Bending fluctuations of semiflexible rods are significantly affected by entanglement only above a concentration  $c^{**}$ , where  $c^{**} \sim 10^3 L^{-3}$  for chains of similar length  $L$  and persistence length. For  $c > c^{**}$ , the tube radius  $R_e$  approaches a dependence  $R_e \propto c^{-3/5}$ , and the linear viscoelastic response develops an elastic contribution that is absent for  $c < c^{**}$ . Experiments on isotropic solutions of F-actin span concentrations near  $c^{**}$  for which the predicted asymptotic scaling of the plateau modulus  $G \propto c^{7/5}$  is not yet valid.

Solutions of long polymers become entangled when the concentration or chain length exceeds a threshold. The nature of “entanglement” is obviously different, however, for random walks, rigid rods, and semiflexible threads. It has been proposed that solutions of semiflexible rods, of length  $L$  less than or equal to their persistence length  $L_p$ , may exhibit two different levels of entanglement, in different concentration regimes [1, 2, 3, 4] – a loosely-entangled regime, in which only rotations and transverse translations are hindered by collisions, and a tightly-entangled regime, in which transverse shape fluctuations are also strongly affected. The crossover between these two regimes is expected to be associated with a qualitative change in viscoelastic properties, due to the inability of a tightly-entangled solution to rapidly relax stress arising from transverse chain deformations. Clear experimental evidence of “tight” entanglement has been obtained only for solutions of very long actin protein filaments (F-actin), of length  $L \sim L_p \sim 10\mu\text{m}$  and diameter  $d \sim 10$  nm. The evidence comes both from visualization of fluorescently labelled chains [5, 6] and from rheological measurements [7, 8, 9, 10]. It remains unclear, however, whether bending fluctuations are ever significantly hindered in isotropic solutions of any of a variety of other well-studied model systems of semiflexible rods with  $L \sim L_p$  [11], for which the average chain lengths and aspect ratios are all much smaller than those obtainable with F-actin. Simulations offer a potentially important complement to the experimental study of these systems, which provide access to different information and are subject to different difficulties than those encountered in experiments.

Consider a solution of thin semiflexible rods, each of contour length  $L$  and persistence length  $L_p$ , with  $L \lesssim L_p$ . Let  $c$  be the number density of polymers and  $\rho \equiv cL$  be the contour length per volume. Simple geometrical arguments suggest the following sequence of concentration regimes [4]: At dilute concentrations  $c < c^*$ , where  $c^* \propto L^{-3}$ , chain motion is essentially unhindered. In the loosely-entangled regime,  $c^* \ll c \ll c^{**}$ , rotations and transverse rigid body translations are strongly hindered, but transverse bending fluctuations are not. In this regime, each chain is trapped in a cylindrical cage or tube of radius  $R_e \sim 1/(cL^2)$  [12]. Above a threshold  $c^{**} \sim \sqrt{L_p/L} c^*$ , this cage become narrow enough to also hinder thermal bending fluctuations [1, 2, 3, 4]. At concentrations  $c \gg c^{**}$ , chain motion can be described by

a modified tube model [2, 3, 13] in which each chain undergoes reptation in a narrow wormlike tube. A scaling argument due to Odijk and Semenov [1, 3, 4] predicts a tube radius  $R_e \propto L_p(\rho L_p^2)^{-3/5}$  for  $c \gg c^{**}$

Our simulations use a novel algorithm that was designed to allow simulation of Brownian dynamics of arbitrarily thin but uncrossable wormlike threads. Each polymer is represented as a discretized chain of  $N$  inextensible rods and  $N + 1$  beads. A periodic cubic simulation cell is initially populated with a thermally equilibrated solution of wormlike chains, by a Monte Carlo growth algorithm. At each step of our dynamical simulation, a trial move is generated for a randomly chosen chain by taking one time step of the Brownian dynamics (BD) algorithm used in previous work on dilute solutions [14, 15, 16]. A trial move is rejected, however, if it would cause the chosen chain to cut through any other. Whether or not a move is accepted, another chain is then chosen at random, and the process is repeated. In this work, we use an algorithm for chains with anisotropic friction, with  $\zeta_{\parallel}/\zeta_{\perp} = 1/2$  [16], where  $\zeta_{\parallel}$  and  $\zeta_{\perp}$  are longitudinal and transverse friction coefficients, respectively. Details of the algorithm are presented elsewhere [17, 18]. Here, we present results for entangled solutions of chains with  $L/L_p = 0.25 - 2.0$  and  $N = 10 - 40$  rods at concentrations  $cL^3 = 0 - 4000$ . A 1 mg/ml solution of (hypothetically) monodisperse F-actin filaments with  $L = 8\mu\text{m}$  would have  $cL^3 \simeq 2500$ .

To characterize the effect of entanglement upon bending fluctuations, we have calculated two measures of the transverse mean-squared displacement (MSD) vs. time for the middle bead of a polymer. The quantity  $\langle \Delta d^2(t) \rangle$ , shown in the main plot in Figure 1, is the variance of the distance  $\Delta d(t)$  between the middle bead at time  $t$  and the closest point on the contour of the same chain at an earlier time  $t = 0$ . The inset shows  $\langle \Delta \mathbf{r}_{m,\perp}^2(t) \rangle \equiv \langle |\mathbf{r}_{m,\perp}(t) - \mathbf{r}_{m,\perp}(0)|^2 \rangle$ , in which  $\mathbf{r}_{m,\perp}(t)$  is the transverse component (transverse to the local chain tangent) of the displacement of the middle bead from the chain’s center of mass. The quantity  $\langle \Delta \mathbf{r}_{m,\perp}^2(t) \rangle$  is not sensitive to center-of-mass diffusion, but only to displacements arising from bending fluctuations, and so approaches a finite value at long times. At early times, both measures of transverse MSD increase as  $t^{3/4}$ , as predicted [19]. With increasing concentration, both quantities become suppressed over a range of intermediate times, indicating the formation of a tube.

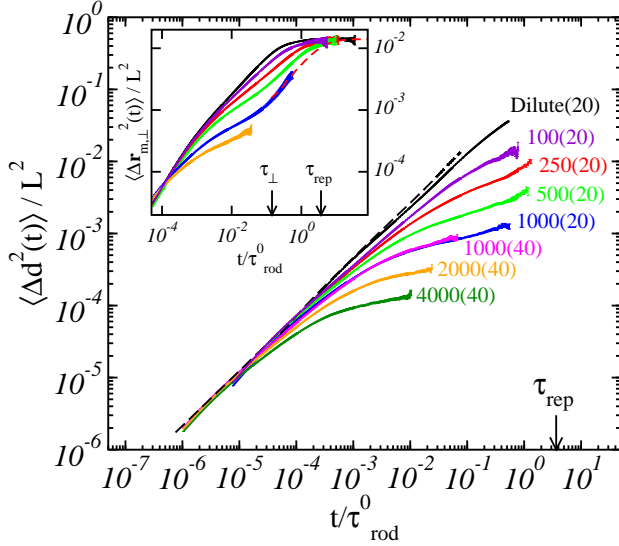


FIG. 1:  $\langle \Delta d^2(t) \rangle / L^2$  vs  $t / \tau_{rod}^0$  for chains with  $L = L_p$ , where  $\tau_{rod}^0 \equiv \zeta_{\perp} L^3 / (72k_B T)$  is the rod rotation time in dilute solution. Numbers near curves are values of  $cL^3$  (or 'Dilute' for  $c = 0$ ), while numbers in parentheses indicate  $N$ . The black dashed line is the predicted asymptote at early times, for which  $\langle \Delta d^2(t) \rangle \propto t^{3/4}$ . Inset:  $\langle \Delta r_{m,\perp}^2(t) \rangle$  vs  $t / \tau_{rod}^0$  for  $L = L_p$  and  $cL^3 = \text{'Dilute'}, 100, 250, 500, 1000, \text{and } 2000$ . The red dashed line is the result of a slithering-snake simulation of pure reptation. [18]

If each chain were confined to a tube of well-defined radius  $R_e$  over a wide range of intermediate times,  $\langle \Delta d^2(t) \rangle$  would develop a plateau, with a plateau value  $\langle \Delta d^2(t) \rangle \simeq 4R_e^2$ . Here,  $R_e^2$  is defined, as in Ref. [20], as the variance of the transverse displacement of the chain from the ‘‘center’’ of the tube (i.e., the average chain contour) in either of two transverse directions. A plateau could appear in  $\langle \Delta d^2(t) \rangle$  even in the rigid rod limit, however, due to suppression of transverse center-of-mass motion. The suppression of  $\langle \Delta r_{m,\perp}^2(t) \rangle$  at intermediate times, however, is evidence of hindered *bending* motion, and thus of tight entanglement. In fact, we never observe a clean plateau in either quantity. Instead, we see a crossover from  $t^{3/4}$  growth at small  $t$  to a much slower growth at intermediate times, which becomes flatter with increasing concentration and/or chain length (i.e., increasing  $cL^3$ ), with a crossover time  $\tau_e$  that decreases with increasing  $c$ . The suppression in  $\langle \Delta r_{m,\perp}^2(t) \rangle$  is significant only for  $cL^3 \gtrsim 500$ , suggesting a crossover  $c^{**} \simeq 500/L^3$  for  $L = L_p$ .

For  $cL^3 = 1000$ , our results for  $\langle \Delta r_{m,\perp}^2(t) \rangle$  include both a plateau at intermediate times and an upturn at the end of this plateau. This upturn is mimicked very accurately by the results of a separate slithering-snake simulation of pure reptation of a wormlike chain (the red dashed line in the inset) [18]. Pure reptation yields a nonzero transverse MSD  $\langle \Delta r_{m,\perp}^2(t) \rangle$  at times less than the reptation time  $\tau_{rep} = \zeta_{\parallel} L^3 / (\pi^2 k_B T)$  because reptation occurs along a curved tube.  $\langle \Delta d^2(t) \rangle$  is defined so as not to be affected by pure reptation, and shows a slightly broader plateau than  $\langle \Delta r_{m,\perp}^2(t) \rangle$ .

To quantify  $\tau_e$  and  $R_e$ , we have collapsed our data for  $\langle \Delta d^2(t) \rangle$  in a manner that assumes the existence of a scaling

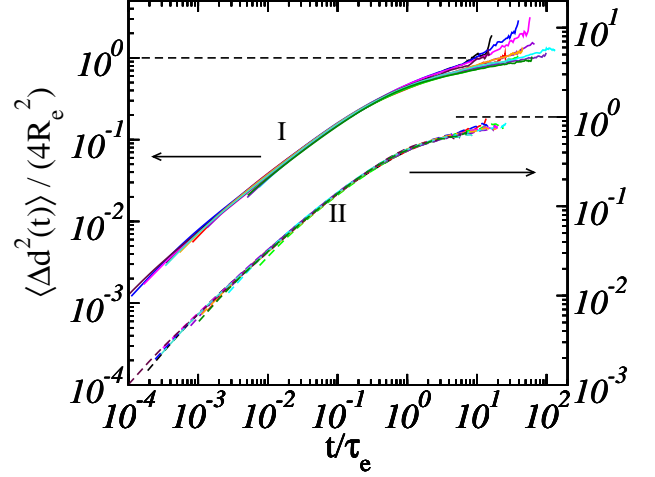


FIG. 2: Collapse of  $\langle \Delta d^2(t) \rangle$  data. Curves labelled ‘‘I’’ represent collapse of data for  $N = 20$ ,  $cL^3 = 250, 500, 1000$ , and  $L/L_p = 0.25, 0.5, 1.0, 2.0$ . Curves labelled ‘‘II’’ represent collapse of data for  $N = 40$ ,  $cL^3 = 1000, 2000, 4000$ , and  $L/L_p = 0.25, 0.5, 1.0, 2.0$ .

relationship  $\langle \Delta d^2(t) \rangle = 4R_e^2 f(t / \tau_e)$ . That is, we have chosen values for  $R_e$  and an entanglement time  $\tau_e$  for each set of parameters so as to collapse the data for many different values of  $L/L_p$  and  $cL^3$  onto a master curve of  $\langle \Delta d^2(t) \rangle / (2R_e)^2$  vs.  $t / \tau_e$ . The resulting collapse is shown in Figure 2. We display separate master curves for chains with  $N = 20$  and  $N = 40$  because early time behavior is noticeably different for discrete chains with different numbers of rods. The collapse is excellent for solutions with  $cL^3 \geq 1000$ . The horizontal dashed lines with  $\langle \Delta d^2(t) \rangle / 4R_e^2 = 1$  represent an assumed long time asymptote for hypothetical systems of much longer chains, from which we have extracted estimates of  $R_e$ .

Figure 3 shows resulting values of the dimensionless tube radius  $R_e/L_p$  vs. dimensionless concentration  $\rho L_p^2$  for systems with  $L/L_p = 0.25 - 2.0$ . Dimensional analysis requires that the ratio  $R_e/L_p$  be a function  $R_e/L_p = f(\rho L_p^2, L/L_p)$  of dimensionless length  $L/L_p$  and dimensionless concentration  $\rho L_p^2$  alone. In the tightly-entangled regime, however, we expect  $R_e$  to become independent of  $L$ , implying that  $R_e/L_p$  must approach a function of  $\rho L_p^2$  alone for  $c \gg c^{**}$ . At high concentrations, our results for different values of  $L/L_p$  do indeed approach a common asymptote, which is furthermore very accurately described by the predicted relation  $R_e/L_p = \alpha(\rho L_p^2)^{-3/5}$ , with  $\alpha = 0.95$  (dashed black line). For each value of  $L/L_p$ ,  $R_e/L_p$  also exhibits small but systematic deviations from this asymptote at lower concentrations. This deviation is seen most clearly in the inset, in which we plot the ratio  $R_e / [0.95 L_p (\rho L_p^2)^{-3/5}]$  vs.  $c / c^{**}$ , where we have taken  $c^{**} = 500 L_p^{1/2} L^{-7/2}$ . The near collapse of the deviations from the asymptote for the stiffest 2 chains ( $L/L_p = 0.25$  and  $0.5$ ) is consistent with the prediction that  $c^{**} \propto L_p^{1/2} L^{-7/2}$  for  $L \ll L_p$ . [4]. The experimental values for  $R_e$  in F-actin solutions (crosses) are the fluorescence microscopy results of Käs *et al.* [5, 6], as defined and presented previously in Ref. [20].

The crossover from loose- to tight-entanglement is expected

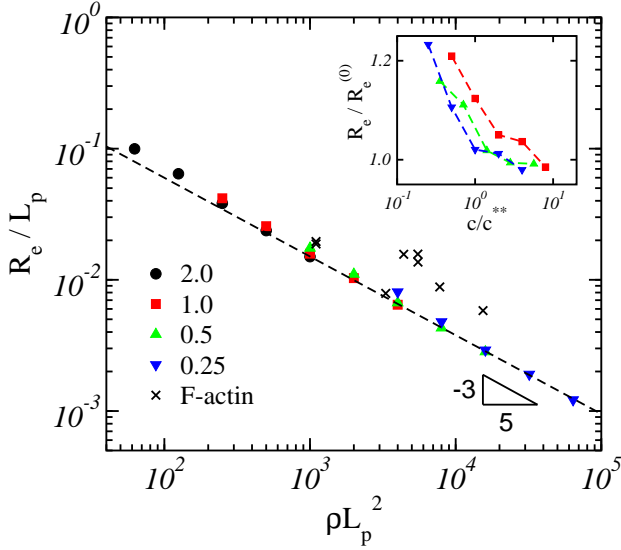


FIG. 3: Non-dimensionalized tube radius vs. concentration. Numbers in the legend are values of  $L/L_p$ . Crosses are fluorescence microscopy results for  $F$ -actin [5, 6], non-dimensionalized by  $L_p = 17\mu m$ . Inset: Deviation  $R_e/R_e^{(0)}$  from the asymptote vs.  $c/c^{**}$ , where  $R_e^{(0)} \equiv 0.95L_p(\rho L_p^2)^{-3/5}$  corresponds to the dashed line in the main plot, and where  $c^{**} = 500L_p^{1/2}L^{-7/2}$ .

to cause a dramatic change in viscoelastic behavior. Detailed theories of linear viscoelasticity have been developed for the extreme limits of dilute solutions ( $c \ll c^*$ ) [14, 15] and of very tightly entangled solutions ( $c \gg c^*$ ) [13]. Both theories make use of a formal decomposition of the stress into curvature, orientational, and tension contributions [4], and a corresponding decomposition of the dynamic modulus  $G(t)$  (i.e., the response to an infinitesimal step strain) as a sum  $G(t) = G_{\text{curv}}(t) + G_{\text{ornt}}(t) + G_{\text{tens}}(t)$ . In both dilute and loosely-entangled solution,  $G_{\text{curv}}(t)$  and  $G_{\text{tens}}(t)$  are predicted to exhibit power law decays at very early times, but to decay exponentially at times greater than the relaxation time  $\tau_{\perp} = \beta\zeta_{\perp}L^4/(k_B T L_p)$  of the longest wavelength bending mode, where  $\beta = (4.74)^{-4}$ . For  $c < c^*$ ,  $G(t)$  is thus dominated at  $t > \tau_{\perp}$  by a more slowly decaying orientational modulus  $G_{\text{ornt}}(t) \simeq (3/5)ck_B T e^{-t/\tau_{\text{rod}}}$ , where  $\tau_{\text{rod}}$  is a rotational diffusion time. In loosely-entangled solutions, the only predicted effect of entanglement is to increase  $\tau_{\text{rod}}$ , without significantly changing  $G_{\text{curv}}(t)$  or  $G_{\text{tens}}(t)$ . The plateau of magnitude  $(3/5)ck_B T$  in  $G_{\text{ornt}}(t)$ , which is present even in dilute solution, reflects the free energy cost of partially aligning an initially random distribution of rod orientations. The crossover to tight entanglement, however, is expected to cause a plateau to appear in  $G_{\text{curv}}(t)$ , with a plateau value  $G_{\text{curv},0}$  that varies as [4, 13, 21]  $G_{\text{curv},0} \propto k_B T \rho^{7/5} L_p^{-1/5}$  for  $c \gg c^*$ .

We have “measured”  $G(t)$  and its components by simulating stress relaxation after a rapid, small amplitude uniaxial step extension of an initially cubic periodic unit cell. Stress is evaluated using the virial tensor, as in previous simulations of dilute solutions [14, 15]. Measurements of  $G(t)$  in dilute solution by this method agree to within statistical errors with

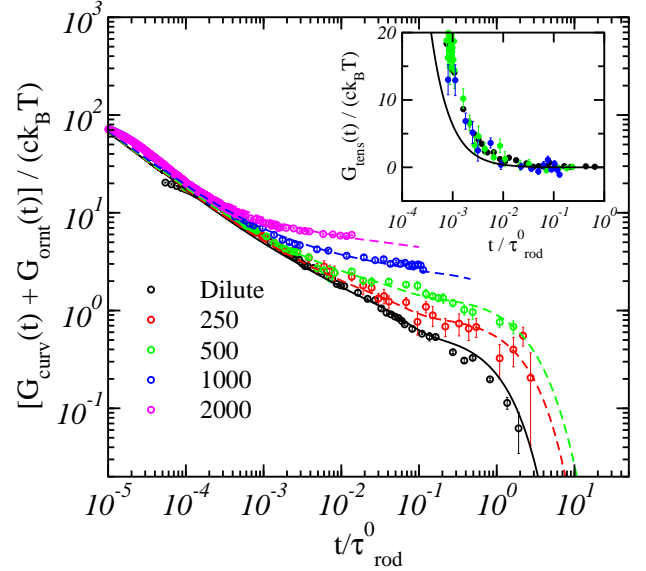


FIG. 4: Non-dimensionalized sum  $[G_{\text{ornt}}(t) + G_{\text{curv}}(t)]/(ck_B T)$  of the orientational and curvature moduli vs  $t/\tau_{\text{rod}}^0$  for  $L/L_p = 0.5$ . Numbers in the legend are values of  $cL^3$ . Dashed curves are fits, as discussed in the text. Black solid curves in both plots are theoretical predictions for dilute solutions [15]. Inset: Corresponding tension stress  $G_{\text{tens}}(t)/(ck_B T)$  for systems with  $cL^3 = 0, 250, 500, 1000$ .

those obtained previously [14, 15] from stress fluctuations in equilibrium.

In Figure 4, the main plot shows a non-dimensionalized sum  $[G_{\text{ornt}}(t) + G_{\text{curv}}(t)]/(ck_B T)$  of the two components of  $G(t)$  that are predicted and observed to exhibit an elastic plateau. The inset shows  $G_{\text{tens}}(t)/(ck_B T)$ , which, as expected [13], does not exhibit a plateau, and which is found to be almost independent of  $c$  over this range of parameters. The plateau in  $[G_{\text{ornt}}(t) + G_{\text{curv}}(t)]/(ck_B T)$  becomes significantly greater than the limiting value of  $3/5$  obtained in dilute solution, which arises from  $G_{\text{ornt}}(t)$  alone, only above an apparent crossover concentration of  $c^{**}L^3 \sim 250 - 500$ , above which  $G_{\text{curv}}(t)$  also begins to contribute to the observed plateau. The terminal relaxation is accessed in our simulations only for  $cL^3 \leq 500$ , but the plateau value is always accessible.

To quantify the plateau modulus, we have fit the sum  $G_{\text{curv}}(t) + G_{\text{ornt}}(t)$  to a function

$$\frac{3}{5}ck_B T e^{-t/\tau_{\text{rod}}} + G_{\text{curv,dil}}(t) + G_{\text{curv},0} e^{-t/\tau_0} \quad (1)$$

Here, the first term on the r.h.s. is an expression for  $G_{\text{ornt}}(t)$ , where  $\tau_{\text{rod}}$  is a concentration-dependent rotational diffusion time, and  $G_{\text{curv,dil}}(t)$  is the prediction of Shankar et al. for  $G_{\text{curv}}(t)$  in dilute solution. The quantity  $G_{\text{curv},0}$  is the contribution of  $G_{\text{curv}}(t)$  to the overall plateau modulus, which is an adjustable parameter. We have used a time constant  $\tau_0 = \tau_{\text{rep}}/2$  for the relaxation of the curvature plateau. This was chosen to fit the observed decay of  $G_{\text{curv}}(t)$  alone (not shown separately here) at  $cL^3 = 250$  and  $500$ , and is consistent with a double-reptation model of the relaxation of the

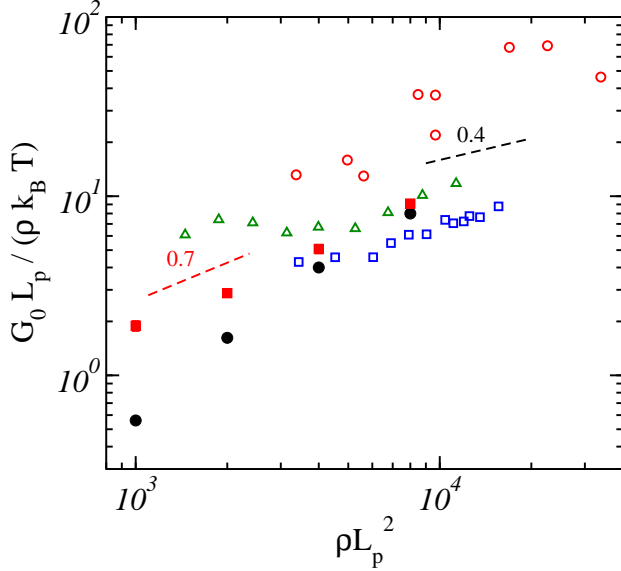


FIG. 5:  $(G_0 L_p)/(\rho k_B T)$  vs  $\rho L_p^2$  from simulations and experiments on entangled F-actin solutions. Simulation results for systems with  $L/L_p = 0.5$  are shown for both  $G_0$  (filled squares) and  $G_{\text{curv},0}$  (filled circles). Experimental results for F-actin solutions of Gardel *et al.* [10] (open circles) and of Hinner *et al.* [8] for filaments of unregulated length (open triangles) and of average length  $16\mu\text{m}$  regulated by gelsolin (open squares). Dashed line with a slope of 0.4 is the prediction of the binary collision approximation of Ref. [20].

curvature plateau. Values of the rotational diffusion time  $\tau_{\text{rod}}(c)$  were measured in separate equilibrium simulations [17], which yield  $\tau_{\text{rod}}/\tau_{\text{rod}}^0 = (2.10, 3.06, 4.46, 6.17)$  for  $cL^3 = (250, 500, 1000, 2000)$ . The values of  $G_{\text{curv},0}$  obtained by fitting this data depend very little upon our choices for the time constants  $\tau_0$  and  $\tau_{\text{rod}}(c)$ .

The total plateau modulus  $G_0$  in  $G(t)$  is a sum  $G_0 = (3/5)ck_B T + G_{\text{curv},0}$  of orientational and curvature contributions. Figure 5 compares simulation results for  $G_0$  and  $G_{\text{curv},0}$  to reported values of  $G_0$  in entangled F-actin solutions [8, 10]. The results of Hinner *et al.* [8] were obtained by macroscopic rheological measurements, while those of Gardel *et al.* [10] were obtained from two-particle micro-rheology. Our results for  $G_0$  agree well with the values of Hinner *et al.*, and are well within the scatter of results reported in the recent literature. A fit of our results for  $G_0$  to a power of  $c$  yields  $G_0/c \propto c^{0.7}$ .

It is clear from the simulation data, however, that the range of concentrations accessed in our simulations, and most of that studied experimentally, lies within about one decade of the beginning of a broad crossover to tightly entangled behavior, below which  $G_{\text{curv}}(t)$  does not contribute to  $G_0$ . As a result of this proximity to  $c^{**}$ ,  $G_{\text{ornt}}(t)$  dominates  $G_0$  over much of this range, while the contribution  $G_{\text{curv},0}$  that is actually predicted to vary as  $G_{\text{curv},0}/c \propto c^{0.4}$  in the limit  $c \gg c^{**}$  increases much more rapidly from nearly zero. The results suggest that the very rough agreement between the predicted asymptotic behavior of  $G_{\text{curv},0}$  for  $c \gg c^{**}$  and measurements of  $G_0$  in F-actin may be largely fortuitous.

The isotropic-nematic (IN) transition for rodlike polymers occurs at a concentration  $c_{\text{IN}}L^3 \simeq 4L/d$ . Values of  $L/d$  for

available model systems with  $L \lesssim L_p$  other than F-actin, such as Fd virus [22] ( $L \simeq 0.9\mu\text{m}$ ,  $L_p \sim 2\mu\text{m}$ ,  $d \sim 7\text{ nm}$ ) and rod-like poly(benzyl glutamate) [11] ( $L_p \sim 0.15\mu\text{m}$  and  $d \sim 2\text{ nm}$ ) are all at least 10 times smaller than for F-actin, for which  $L/d \sim 10^3$ . The IN transition in systems with  $L/d < 100$  occurs at concentrations  $c_{\text{IN}}L^3 \lesssim 400$ , at which  $c < c^{**}$ . Our rough estimate of  $c^{**} \sim 500L_p^{1/2}L^{-7/2}$  for  $L \lesssim L_p$  implies that a clear tightly-entangled isotropic regime for semiflexible rods can exist only in systems with  $L/d \gtrsim 10^3$ . This is consistent with the fact that a clear rheological signature of tight entanglement has been observed only in F-actin solutions.

Taken as a whole, our results both provide evidence for the correctness of a simple scaling theory for the asymptotic dependence of tube radius upon concentration in tightly-entangled solutions, and (equally importantly) clarify the limits of validity that theory, particularly as applied to rheology. It appears that bending fluctuations of rods with  $L \sim L_p$  are significantly hindered by entanglement only under surprisingly stringent conditions.

This work has been supported by ACS Petroleum Research Fund grant 38020-AC7, using computer resources provided by the Minnesota Supercomputer Center and the Univ. of Minnesota NSF MRSEC.

\* Electronic address: morse@cems.umn.edu

- [1] T. Odijk, *Macromolecules* **16**, 1340 (1983).
- [2] M. Doi, *J. Polym. Sci., Polym. Symp.* **73**, 93 (1985).
- [3] A. N. Semenov, *J. Chem. Soc., Faraday Trans. 2* **82**, 317 (1986).
- [4] D. C. Morse, *Macromolecules* **31**, 7030 (1998).
- [5] J. Käs, H. Strey, and E. Sackmann, *Nature* **368**, 226 (1994).
- [6] J. Käs, H. Strey, J. X. Tang, D. Finger, R. Ezzell, E. Sackmann, and P. A. Janmey, *Biophys. J.* **70**, 609 (1996).
- [7] M. Sato, G. Leimbach, W. H. Schwarz, and T. D. Pollard, *J. Biol. Chem.* **260**, 8585 (1985).
- [8] B. Hinner, M. Tempel, E. Sackmann, K. Kroy, and E. Frey, *Phys. Rev. Lett.* **81**, 2614 (1998).
- [9] F. G. Schmidt, B. Hinner, and E. Sackmann, *Phys. Rev. E* **61**, 5646 (2000).
- [10] M. L. Gardel, M. T. Valentine, J. C. Crocker, A. R. Bausch, and D. A. Weitz, *Phys. Rev. Lett.* **91**, 158302 (2003).
- [11] T. Sato and A. Teramoto, *Adv. Polym. Sci.* **126**, 85 (1996).
- [12] M. Doi, *J. de Physique* **36**, 607 (1975).
- [13] D. C. Morse, *Macromolecules* **31**, 7044 (1998).
- [14] M. Pasquali, V. Shankar, and D. C. Morse, *Phys. Rev. E* **64**, 020802 (2001).
- [15] V. Shankar, M. Pasquali, and D. C. Morse, *J. Rheol.* **46**, 1111 (2002).
- [16] A. Montesi, M. Pasquali, and D. C. Morse, *J. Chem. Phys.* **122**, 084903 (2005).
- [17] S. Ramanathan, Ph.D. thesis, University of Minnesota (2006).
- [18] S. Ramanathan and D. C. Morse, *J. Chem. Phys.* (in press) (2007), arxiv:cond-mat/0610473.
- [19] R. Granek, *J. Phys. II* **7**, 1761 (1997).
- [20] D. C. Morse, *Phys. Rev. E* **63**, 031502 (2001).
- [21] H. Isambert and A. C. Maggs, *Macromolecules* **29**, 1036 (1996).
- [22] F. G. Schmidt, B. Hinner, E. Sackmann, and J. X. Tang, *Phys. Rev. E* **62**, 5509 (2000).